Materials Research. 2016; 19(6): 1286-1291
DOI: http://dx.doi.org/10.1590/1980-5373-MR-2016-0210

Grain-Boundary Resistance and Nonlinear Coefficient Correlation for SnO_2-Based Varistors

Mateus Gallucci Masteghin[a], Marcelo Ornaghi Orlandi[a]*

[a]Chemistry Institute, São Paulo State University, Araraquara, SP, Brazil

Received: March 09, 2016; Revised: June 27, 2016; Accepted: August 23, 2016

This work has focused on the electrical and microstructural properties of Nb_2O_5-doped SnO_2-MnO_2 ceramics. The pellets were prepared by solid-state reaction method according to the system (99.5-x) SnO_2 - 0.5 MnO_2 - x Nb_2O_5, on the following molar ratio x = 0.05; 0.10; 0.15; 0.20 and 0.25. Scanning electron microscopy and electrical measurements (*ac* and *dc*) were used to study the materials properties. The results showed that the increase of Nb_2O_5 content in the SnO_2-MnO_2 matrix has led to an increase in the varistor properties. A detailed study of the electrical properties of materials was conducted using impedance spectroscopy and the results indicated that Nb_2O_5 has a tendency to form an electron trapping level near the conduction band. In order to explain these findings, a parallel equivalent circuit model was used to simulate the values of the grain boundary resistance. A close relationship was found between the value of the nonlinear coefficient and the grain boundary resistance for the studied varistors, where both values increased with increasing the amount of Nb_2O_5, which is important for practical applications.

Keywords: *Varistor, Tin oxide, Electrical properties, Impedance spectroscopy*

1. Introduction

Semiconductor Metal Oxides (SMO)[1] are interesting materials due to their nonlinear electrical response, making their use possible in many technological applications, such as light and gas sensors, electro-optical devices, photovoltaic cells, and electrical transient suppressors (varistors), responsible for acting as an energy drain.

This characteristic is due to the polycrystalline nature of ceramic varistors and the effective potential barriers at the grain boundaries that enables a nonlinear relationship between the voltage and the current. This non-ohmic behavior of the ceramics has been defined by the empirical equation:

$$I = K \cdot V^{\alpha} \quad (1)$$

in which I is the current, V is the applied voltage, K is a constant related to the microstructure of the material and α is the nonlinear coefficient.

In varistor materials, one of the most important parameter is the nonlinear coefficient (α). The value of α defines how fast the change is from the high resistive to the low resistive state, allowing the excess current to flow through the ground. Another important parameter is the breakdown electric field (E_b) which determines the practical application of varistor, i.e., low, medium or high voltage networks. Since these electronic ceramics are used directly connected to a voltage source in parallel with the circuit element being protected, E_b values are selected slightly above the working voltage of the circuit element. Finally, another factor that should be taken into account is the leakage current (I_l), which is the current flowing through the circuit when the voltage is 80% of the breakdown voltage. There has been a correlation between the leakage current and the efficiency of the electrostatic potential barrier[2], which may allow the current flux by tunneling and/or thermionic emission before reaching the breakdown voltage, which results in functional losses in the circuit.

A wide variety of materials have been employed to obtain the varistor behavior, like ZnO[3,4,5,6,7], SnO_2[8,9], TiO_2[10], and more recently $CaCu_3Ti_4O_{12}$[11], and it has been shown that the non-ohmic characteristic is related to the back-to-back Schottky type barrier located at the grain boundary region[12,2]. This barrier is formed during the sintering process due to oxygen enrichment at grain boundaries compensated by interstitial cations and/or oxygen vacancies in the adjacent region[13].

The tin oxide is an n-type semiconductor as a consequence of the oxygen non-stoichiometry, enabled by the coordination 6:3 in the rutile-type crystalline structure[14,15]. It has been shown that tin dioxide is a strong candidate to replace the commercial zinc oxide varistors[8], presenting some advantages, such as the need for a small amount of dopants to obtain similar non-ohmic properties (high nonlinear coefficient and low leakage current), single phase pattern at the detection limit of X-ray diffraction technique, higher thermal conductivity that enables better mechanical stability during a voltage overload, and much greater chemical inertness; i.e., SnO_2 is not attacked by acids or weak bases and thus can be used in harsh environments without any previous preparation.

* e-mail: orlandi@iq.unesp.br

However, pure SnO_2 usually presents low density even when sintered at high temperatures[16]. To overcome this obstacle for the application as a varistor system, Park et al.[17] proposed a sintering at 1400 degrees for 12 hours under an isostatic pressure of 150 MPa, yielding 97% of densification. Another alternative was proposed by Cerri et al.[18], who studied the addition of CoO and MnO_2 to the tin oxide matrix, reaching 97% or more of the theoretical density using low amount of dopants and lower sintering temperatures (1300 ºC). Less common is the use of CaO, wherein the Ca with high ionic radius (100 pm compared to 75.0 pm and 83.0 pm of the Co^{+2} and Mn^{+2}, respectively) has low solubility in the tin oxide matrix, segregating at the SnO_2 grain boundaries, which might decrease the grain boundary mobility, leading to a decrease in the average grain size[19]. The densification of tin dioxide is promoted by the oxygen vacancy formation during sintering, which controls the grain boundary mobility and decreases the vapor pressure of tin oxide. Thus, the densification is controlled by the densifying mechanisms that prevail over the non-densifying ones, as evaporation/condensation or neck formation between the grains.

In recent studies, the SnO_2-MnO_2-Nb_2O_5 varistor system has been found to present good electrical properties[20]. Therefore, we chose to carry out an in-depth study using impedance spectroscopy, once the typical varistor parameters can be obtained by *dc* measurements and this type of analysis only provides the global resistance of the studied sample. Hence, impedance measurements are important because the diffusivity of the charge carriers across grain boundaries, trap levels, grains and electrodes has different relaxation times when an alternating electrical excitation is applied to the material and, therefore, each resistance can be separated in the frequency domain. The response times are longer for interactions at the electrode-ceramic interface than to the phenomena that occur in the grain boundary region, which in turn are longer than the phenomena that occur inside the grains. In addition, because this technique is sensitive to microstructural variations, it allows a correlation between the electrical and microstructural properties in the studied materials.

In light of the above, the aim of this work is to present a detailed study of *dc* and *ac* current responses in Nb_2O_5 doped SnO_2-MnO_2 varistor system using *I-V* and impedance spectroscopy measurements as a tool to separate the different resistance contributions present in varistors. Moreover, an attempt to find evidences for a correlation between the material resistance and the varistor characteristics was performed.

2. Experimental Procedure

The samples were prepared using the solid state reaction method, in which the powders, in the correct stoichiometry, were homogenized using the ball milling process (with yttrium stabilized zirconium balls) in alcohol medium for 24 h. The oxides used were SnO_2 (Aldrich), MnO_2 (Aldrich) and Nb_2O_5 (Aldrich), all of them with a purity of 99.9% or more. The composition studied was (99.5-x)SnO_2 - (0.5) MnO_2 - (x)Nb_2O_5, with x = 0.05, 0.10, 0.15, 0.20 and 0.25, in molar percentages, hereinafter called $SnMnNb_x$, with their respective x values. The samples were first compacted in cylindrical discs, 1.0 mm thick and 7.0 mm in diameter, by uniaxial pressing (10 MPa), followed by isostatic pressing at 150 MPa. Next, the samples were sintered at 1305 ºC for 2 hours, with a heating and cooling rate of 10 ºC.min^{-1}, in air atmosphere.

The sintered samples were structurally characterized by X-ray diffraction (XRD, Rigaku, model RINT 2000) using Cu$K\alpha$ radiation. The morphological study of samples was conducted by scanning electron microscopy (SEM-FEG -JEOL, model 7500F) and dual beam microscopy (FIB -FEI, model Helios NanoLab 600i), equipped with X-ray energy dispersive spectroscopy (EDS) detector. The average grain size was calculated based on the linear intercept[21] method taken into account at least 200 grains of each composition.

In order to take electrical measurements, silver contacts were placed on the parallel polished surfaces of samples, and were heated at 80 °C for 2 hour in air atmosphere to eliminate the organic solvents. The direct current (*dc*) measurements were performed in a stabilized high voltage source-meter unit (Keithley, model 237), using the voltage range from 0 to 1100 V, with step of 20 V, and a current compliance of 10 mA. Impedance spectroscopy analyses were carried out using a frequency response analyzer (FRA32M - Autolab, model PGSTAT), in the frequency range from 10 mHz to 1 MHz, and amplitude of 500 mV. The results were analyzed by the NOVA 1.10 software and the Equivalent Circuit (EQUIVCRT) program[22,23]. Based on the electrical response of materials and the physical interpretation of systems, equivalent circuits were proposed for each varistor composition and the simulated values were compared to the experimental ones in a fit at the complex plane.

3. Results and Discussion

After the sintering process, the samples were structurally characterized by X-ray diffraction (not shown here), and only the cassiterite phase of SnO_2 was observed for all compositions. This result was predictable since the dopants used in this work are in the amount below the detection limit of XRD equipment.

Figure 1 shows FEG-SEM images of all sintered samples, and Table 1 presents the values of average grain size and the relative density of pellets. It is possible to observe that all the samples exhibit high relative density, due to the added manganese and its effect on the formation of oxygen vacancies. It is also noted a decrease in the average grain size with increasing the amount of niobium as a result of its action decreasing the grain boundary mobility. Furthermore, SEM

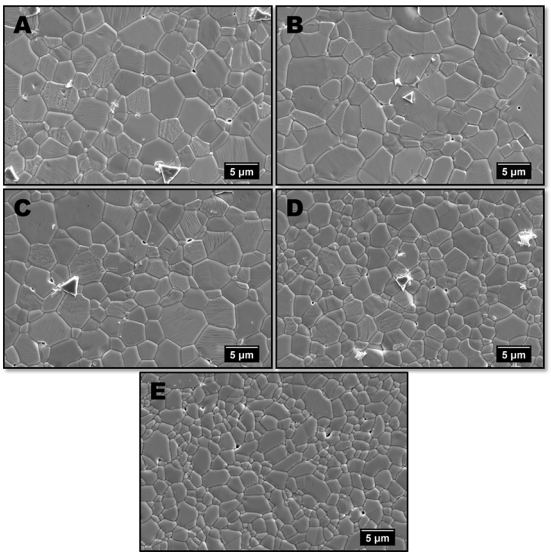

Figure 1. FEG-SEM images of varistor system (99.5-X) SnO_2 - (0.5) MnO_2 - (X) Nb_2O_5, with the following X content: A) 0.05%; B) 0.10%; C) 0.15%; D) 0.20% and E) 0.25%.

Table 1. The calculated average grain size for each varistor system studied.

System	Grain Size (µm)	Relative Density
$SnMnNb_{0.05}$	5.7	98%
$SnMnNb_{0.10}$	5.6	98%
$SnMnNb_{0.15}$	4.7	99%
$SnMnNb_{0.20}$	3.9	99%
$SnMnNb_{0.25}$	3.0	95%

images show that samples have some triangle precipitates at triple points of the grain boundaries, and the amount of precipitates also decreases with increasing the Nb_2O_5 content in the sample.

A detailed study of the precipitates present in the sample $SnMnNb_{0.05}$ was performed in a dual beam microscope equipped with EDS detector. Figure 2 presents the secondary (SE) and backscattered electrons (BSE) image of the sample where it is possible to observe that the material consists of two distinct phases; the bright grains being composed by a phase with average atomic number higher than the dark triangular precipitates. In order to study in more detail the precipitates that are present at triple points, a milling of 8 microns depth was made in the extension of the grain boundary, tangential to the precipitate, using the Ga^{+3} ions source of a dual-beam microscope. Figure 3 presents the SE image of the cross-section showing that the precipitate accompanies the grain boundary in depth. The chemical mapping obtained by EDS proves that precipitates are rich in manganese and oxygen, while grains are mainly composed by tin and oxygen.

At this point, it is worth discussing the importance of microstructure on electrical properties of varistor systems,

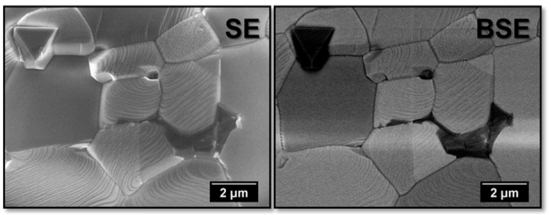

Figure 2. SE and BSE SEM images of triangular precipitates at grain boundary of $SnMnNb_{0.05}$ sample.

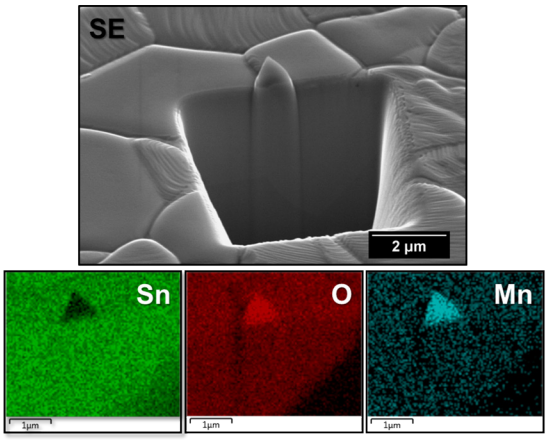

Figure 3. SE image and EDS mapping of a precipitate at the grain boundary. The cut in depth shows the three-dimensional extension of precipitate in the sample.

especially the existence of the precipitates. It is known that for SnO_2 based varistors a homogeneous layer of transition metal segregated at the grain boundary region is fundamental to obtain high nonlinear values (α)[13]; in a similar way to the ZnO based varistors the presence of bismuth oxide phase segregated along the grain boundary is fundamental for its electrical response[24,25]. The SEM and the EDS results for Nb_2O_5-doped SnO_2-MnO_2 varistor system present two phases, or two kinds of SnO_2-SnO_2 grain boundaries, one thin and Mn rich (called type I), and other thick and Mn poor (called type II), and the type I grain boundary is considered desirable to obtain good varistor properties[26].

Thus, in Mn-doped SnO_2 varistors, the manganese is the transition metal responsible for the formation of the potential barrier, and only type I grain boundaries should present effective barriers for electron transport. However, it has been shown that a significant amount of type II grain boundaries are present in the samples (especially those with lower amount of Nb_2O_5) jeopardizing the electrical properties. This loss in the electrical properties happens because the Mn rich precipitates incorporate the manganese which should be homogenously segregated at the grain boundaries. It generates some non-effective potential barriers allowing a free conduction path for electrons, which is responsible for the low nonlinear coefficient and the high leakage current (I_l) values.

The above discussion is corroborated by the results in Figure 4, where the *dc* electrical response of the varistors can be observed by the plot of the electric field as a function of the density of current. All samples present a non-ohmic behavior, but the transition between the resistive states to the conductive one is more abrupt with increasing the Nb_2O_5 content (which is a qualitative measure of α coefficient). Besides, Figure 4 also shows that the breakdown electric field is higher as the amount of niobium increases.

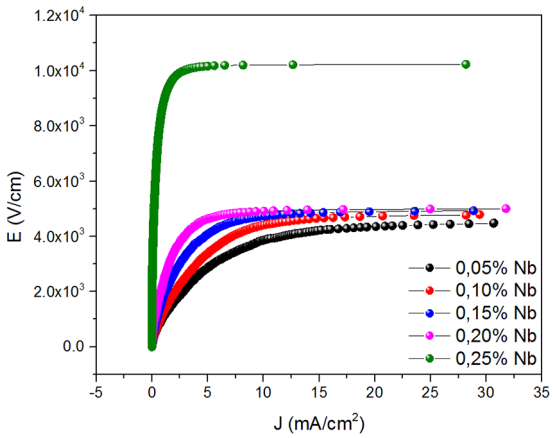

Figure 4. *DC* measurements for all compositions showing that both the breakdown electric field and the nonlinear coefficient increases with the amount of niobium.

The values of the nonlinear coefficient (α) and the breakdown electric field are shown in the Table 2 that also presents the leakage current. One can observe that with increasing the concentration of Nb_2O_5, an increase in the nonlinear coefficient is observed, given the electrons donor characteristic of the Nb_2O_5 substituting SnO_2, increasing the conductivity of the grain. This donor effect can be seen by the reaction represented by the Kroger-Vink notation:

$$2\,Nb_2O_5 \xrightarrow{SnO_2} 4\,Nb_{Sn}^{\cdot} + 10\,O_O^{x} + 4e^{-} \quad (2)$$

Table 2. Varistor characteristics obtained from the *dc* measurements.

$SnMnNb_x$	α	E_b	I_l (μA)
0,05	1.7	1076	231
0,10	3.1	1214	244
0,15	4.2	1788	252
0,20	6.0	2314	203
0,25	11.4	8786	163

It is also possible to note an increase in the value of the breakdown electric field that is associated with both the decrease of the average grain size, that produces more grain boundaries in the pellet, and the decrease of precipitates at triple points, which increases the number of effective potential barriers at the grain boundary.

Since this work is mainly focused on the electrical properties of the varistor systems, impedance spectroscopy measurements were performed allowing to distinguish the contribution of the grain boundary using equivalent circuits to describe physically and mathematically the varistor system[27]. The results obtained from the IS technique can be observed in Figure 5.

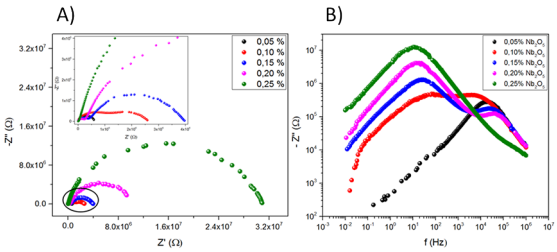

Figure 5. A) Nyquist diagram and B) Imaginary part of resistance *vs.* frequency of all studied $SnMnNb_x$ samples.

It is noticed from Figure 5 that all systems have two semicircles, in which the low frequency semicircle is related to the grain boundary contribution and the high frequency semicircle is related to the electrons trap level[20,28]. The exception is the system $SnMnNb_{0,05}$ which presents only the grain boundary contribution due to the low amount of doping, as clearly observed from Figure 5b[29]. In addition, Figure 5a also shows that the amount of niobium influences the semicircle at high frequency. It is noticeable that increasing the Nb_2O_5 amount produces a decrease in the high frequency semicircle, becoming almost imperceptible for the $SnMnNb_{0,25}$ system. This change in the high frequency impedance data is a consequence of the increase of the charge carriers in the SnO_2 matrix due to the Nb_2O_5 addition.

The proposed equivalent circuit for all varistor systems studied ($SnMnNb_x$) contains a resistor in parallel with a capacitor, both relating to the grain boundary contribution, appointed as R_{gb} and C_{gb}. For the systems doped with more than 0.05% of niobium it was necessary to add in the proposed circuit, in parallel, a capacitor and a constant phase element (in series), appointed as C_t and CPE_t, representing the internal electron trap level. Then, through theoretical simulations using the EQUIVCRT program[21,22] it was possible to obtain only the grain boundary resistance of varistor, since the impedance spectroscopy technique allows the separation of the resistive contribution from the grain boundary and from the trap level. The grain boundary resistance obtained from the simulations for all studied systems is shown in Table 3.

Analyzing the grain boundary resistance and the alpha value it was found that both follow the same tendency as a function of the amount of niobium, shown in Figure 6, which means that increasing the grain boundary resistance it allows

Table 3. Grain boundary resistance through simulations by Equivcrt program for each studied composition.

% Nb_2O_5	R_{gb}
0.05	5.9 x 10^5
0.10	2.6 x 10^6
0.15	3.7 x 10^6
0.20	9.5 x 10^6
0.25	2.9 x 10^7

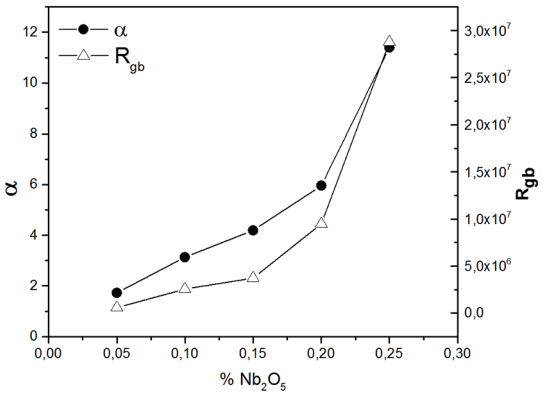

Figure 6. Nonlinear coefficient (left axis) and grain boundary resistance (right axis) as function of Nb_2O_5 content.

for higher values of alpha. This close relation between the alpha and the grain boundary resistance is expected for a varistor when the grain boundary is the key factor for the nonlinear relationship presented by these devices.

This tendency can be explained by taking the derivative of the typical varistor equation: $I = \left(\frac{U}{C}\right)^{\alpha}$, with respect to I, obtaining:

$$\frac{dU(t)}{dI(t)} = \frac{1}{\alpha} \cdot \frac{U}{I} \quad (3)$$

Knowing that $\frac{dU}{dI}$ is the *ac* resistance, given as fix, increasing the grain boundary resistance (related to $\frac{U}{I}$), the nonlinearity coefficient should also increase (1/alpha decreases).

Therefore, to obtain high values of nonlinear coefficient, the material must present a high grain boundary resistance. This makes sense considering the results presented above showing that low amounts of Nb_2O_5 increase the amount of precipitates at triple points generating more non-effective type II potential barriers at grain boundaries and, thus, low alpha values.

It was shown that by combining the results obtained from different characterization techniques we were able to study the $SnMnNb_x$ varistor system in more detail separating the grain boundary and trap level contribution from the global resistance of material. In addition, there is evidence of a close correlation between the grain boundary resistance and the nonlinear coefficient value.

4. Conclusion

In this work the morphological and the electrical properties of Nb_2O_5-doped SnO_2-MnO_2 varistor systems were studied. Varistors are composed of tin oxide grains and exhibit some Mn-rich precipitates at triple points. It was corroborated that precipitates jeopardize the varistor response due to the formation of non-effective potential barriers. Nevertheless, using impedance spectroscopy, it was possible to observe and describe the grain boundary contribution from each system and likewise a correlation between the varistor grain boundary resistance and the nonlinear coefficient was observed. Consequently, in order to obtain higher values of nonlinear coefficient, it is required to ensure a high level of effective potential barriers at the grain boundaries, increasing its resistance and avoiding the leakage current.

5. Acknowledgements

We would like to thank the funding agencies FAPESP (proc. # 2013/07296-2) and CNPq (proc # 402297/2013-0, #447760/2014-9, #800733/2014-2, #303542/2015-2). SEM and FIB facilities were provided by the LMA-IQ-UNESP. We are thankful to Justin Moon for his help revising the manuscript.

6. References

1. Levinson LM, Philipp HR. The physics of metal oxide varistors. *Journal of Applied Physics*. 1975;46(3):1332-1341.

2. Leite ER, Varela JA, Longo E. A new interpretation for the degradation phenomenon of ZnO varistors. *Journal of Materials Science*. 1992;27(19):5325-5329.

3. Matsuoka M. Nonhomic properties of zinc oxide ceramics. *Japanese Journal of Applied Physics*. 1971;10(6):736-746.

4. Mukae K, Tsuda K, Nagasawa I. Non-ohmic properties of ZnO-Rare Earth metal oxide Co_3O_4. *Japanese Journal of Applied Physics*. 1977;16(8):1361-1368.

5. Mukae K. Zinc-Oxide varistors with praseodymium oxide. *American Ceramic Society Bulletin*. 1987;66(9):1329-1331.

6. Mukae K, Tsuda K, Nagasawa I. Capacitance vs voltage characteristics of ZnO varistors. *Journal of Applied Physics*. 1979;50(6):4475-4476.

7. Alim MA, Seitz MA, Hirthe RW. Complex-plane analysis of trapping phenomena in zinc-oxide based varistor grain-boundaries. *Journal of Applied Physics*. 1988;63(7):2337-2345.

8. Pianaro SA, Bueno PR, Olivi P, Longo E, Varela JA. Electrical properties of the SnO_2 - based varistor. *Journal of Materials Science: Materials in Electronics*. 1998;9(2):159-165.

9. Pianaro SA, Bueno PR, Longo E, Varela JA. A new SnO_2 - based varistor system. *Journal of Materials Science Letters*. 1995;14(10):692-694.

10. Yang SL, Wu JM. Effects of Nb_2O_5 in (Ba, Ni, Nb)-added TiO_2 ceramic varistors. *Journal of Materials Research*. 1995;10(2):345-352.

11. Chung SY, Kim ID, Kang SJL. Strong nonlinear current-voltage behaviour in perovskite-derivative calcium copper titanate. *Nature Materials*. 2004;3:774-778.

12. Gupta TK, Carlson WG. A grain boundary defect model for instability/stability of a ZnO varistor. *Journal of Materials Science*. 1985;20(10):3487-3500.

13. Bueno PR, Leite ER, Oliveira MM, Orlandi MO, Longo E. Role of oxygen at the grain boundary of metal oxide varistors: A potential barrier formation mechanism. *Applied Physics Letter*. 2001;79:48-50.

14. Jarzebski ZM, Marton JP. Physical Properties of SnO_2 Materials. I. Preparation and Defect Structure. *Journal of the Electrochemical Society*. 1976;123(7):199C-205C.

15. Jarzebski ZM, Marton JP. Physical Properties of SnO_2 Materials. II. Electrical Properties. *Journal of the Electrochemical Society*. 1976;123(9):299C-310C.

16. Duvigneaud PH, Reighard D. Activated sintering of tin oxide. *Science of Sintering*. 1980;12:287-292.

17. Park SJ, Hirota K, Yamamura H. Densification of nonadittive SnO_2 by hot isostatic pressing. *Ceramics International*. 1984;10(3):116.

18. Cerri JA, Leite ER, Gouvêa D, Longo E, Varela JA. Effect of cobalt(II) oxide and manganese(IV) oxide on sintering of tin(IV) oxide. *Journal of the American Ceramic Society*. 1996;79(3):799-804.

19. Aguilar-Martínez JA, Durán-Régules A, Glot AB, Hernández MB, Pech-Canulf MI, Castillo-Torres J. Effect of CaO on the microstructure and non-ohmic properties of (Co,Sb)-doped SnO_2 varistors. *Revista Mexicana de Física*. 2008;54(1):20-24.

20. Orlandi MO, Bomio MRD, Longo E, Bueno PR. Nonohmic behavior of SnO_2-MnO polycrystalline ceramics. II. Analysis of admittance and dielectric spectroscopy. *Journal of Applied Physics*. 2004;96(7):3811-3817.

21. Shunhua C, Clam D. Characteristic grain size: Part I description and definition. *Journal of Central South University of Technology*. 1997;4(1):20-23.

22. Boukamp BA. A nonlinear least squares fit procedure analysis of immitance data of electrochemical systems. *Solid State Ionics*. 1986;20(1):31-44.

23. Boukamp BA. A package for impedance/admittance data analysis. *Solid State Ionics*. 1986;18-19(Pt 1):136-140.

24. Santhanam AT, Gupta TK, Carlson WG. Microestrutural evaluation of multicomponent ZnO ceramics. *Journal of Applied Physics*. 1979;50(2):852-859.

25. Morris WG, Cahn JW. Adsorption and microphases at grain boundaries in non-ohmic zinc oxide. In: Walter JL, ed. *Grain Boundaries in Engineering Materials*. Claitors: Baton Rouge; 1975.

26. Bueno PR, Orlandi MO, Simões LGP, Leite ER, Longo E, Cerri JA. Nonohmic behavior of SnO_2-MnO polycrystalline ceramics. I. Correlations between microstructural morphology and nonohmic features. *Journal of Applied Physics*. 2004;96(5):2693-2700.

27. Barsoukov E, Macdonald JR, eds. *Impedance Spectroscopy: Theory, Experiment, and Applications*. New Jersey: John Wiley & Sons; 2005. 616 p.

28. Orlandi MO, Bueno PR, Longo E. Influence of thermal annealing treatment in oxygen atmosphere on grain boundary chemistry and non-ohmic properties of SnO_2.MnO polycrystalline semiconductors. *Physica Status Solidi (A)*. 2008;205(2):383-388.

29. Cordado JF, Shim Y, May JE. Bulk electron traps in zinc oxide varistors. *Journal of Applied Physics*. 1986;60(12):4186-4190.